IEEE Access
Multidisciplinary ⋮ Rapid Review ⋮ Open Access Journal

Received September 10, 2021, accepted September 19, 2021, date of publication September 22, 2021,
date of current version September 30, 2021.

Digital Object Identifier 10.1109/ACCESS.2021.3114698

In-Pipe Inspection Robot Capable of Actively Exerting Propulsive and Tractive Forces With Linear Antagonistic Mechanism

F. ITO[1], (Graduate Student Member, IEEE), K. TAKAYA[1], M. KAMATA[1], M. OKUI[1], (Member, IEEE), Y. YAMADA[2], (Member, IEEE), AND T. NAKAMURA[1], (Member, IEEE)

[1]Department of Precision Mechanics, Faculty of Science and Engineering, Chuo University, Bunkyo-Ku, Tokyo 112-8551, Japan
[2]Department of Engineering and Design, Faculty of Engineering and Design, Hosei University, Chiyoda-Ku, Tokyo 102-8160, Japan

Corresponding author: F. Ito (a15.cryr@g.chuo-u.ac.jp)

ABSTRACT In this study, the authors comprehensively evaluated the traveling performance of a flexible pipe inspection robot (PI-RO) that can actively output both propulsion and traction forces. Household pipes must be frequently inspected for cracks and corrosion to ensure continuous provision of water and gas. As these pipes are essential for our everyday life, it is difficult to suspend their usage for long periods; hence, inspection should be conducted for short durations. In addition, inspecting entire pipelines using existing methods is challenging because the pipes are constructed over long distances and have complex structures. Therefore, we developed a flexible robot that can actively output propulsion and traction forces to inspect long-distance complex pipelines, such as household pipelines. Herein, we describe the flexible structural design of a PI-RO that inspects thin one-inch pipes (inner diameter of approximately 28 mm) typically present in household piping. We also evaluated the characteristics of each PI-RO unit. Finally, we confirmed that the PI-RO is not significantly affected by the traveling environment, such as long distances and complex small-diameter pipes, by conducting traveling experiments on small pipes (inner diameter 28 mm) and long-distance (up to approximately 11.7 m) complex pipes composed of horizontal, vertical, and 90° bend pipes.

INDEX TERMS Biomechatronics, inspection, pneumatic systems, pneumatic actuators.

I. INTRODUCTION

Household pipes are essential for the sustenance of urban life. These pipes are employed for long-distance transportation of fluids, such as water and gas, to houses and are placed underground. However, the stable supply of fluids may be hindered when cracks and corrosion occur in the piping over time. To prevent such problems, it is necessary to inspect these pipes frequently. Common household pipe inspection methods include disassembly inspection and nondestructive inspection techniques. As household pipes constitute our everyday living infrastructure, it is difficult to suspend their usage for long periods, and hence, the inspection time for household pipes is limited. Thus, it is difficult to apply the disassembly inspection method to household pipes because the disassembling, inspection, and reassembling processes are extremely time-consuming. In contrast, industrial endoscopes are mainly used for nondestructive inspections [1], [2]. In this method, the operator inserts the endoscope into the piping. As household pipes generally have long and complex structures, large amounts of friction occur between the endoscope and the inner wall of the pipe. Therefore, the pushing force applied by the operator is not sufficiently transmitted to the tip of the industrial endoscope, making the entire process cumbersome. Therefore, a self-propelled endoscope is required for household pipe inspection.

Wheel type [3], [4], snake type [5], [6], cilia vibration type [7], spirochetes type [8], earthworm type [9], [10], and inchworm type [11]–[14], are some examples of self-propelled pipe robots. However, these robots have certain merits and demerits when considering the inspection of the gas pipes that are narrow, complex, and run over long distances. For example, wheel- and snake-type robots can easily move at high speeds, but, owing to their complex and

The associate editor coordinating the review of this manuscript and approving it for publication was Engang Tian.

inflexible structure, downsizing and pushing them through the complex pipes is difficult [15]–[17]. As these robots are driven by electric motors, they must be explosion-proof and waterproof. The explosion-proof functionality renders the downsizing and flexibility of these robots difficult. In contrast, although the cilia vibration and spirochetes types are easy to downsize and have flexible structures, producing high traction forces can be challenging owing to their structural incompetency. Furthermore, these robots may be incapable of traveling through long pipes [7], [8].

Therefore, we have developed a fluid-driven pipe inspection robot (PI-RO) with a small and flexible structure. This robot can travel with high traction forces in the limited space of the pipes. The fluid-driven PI-RO has a fluid-driven actuator, and the mechanical compliance of the actuator enables it to travel along with the shape of the pipe. Fluid-driven PI-ROs are classified into two types: earthworms and inchworms. When the earthworm-type travels inside the pipe, it first expands the anterior body segment in the radial direction and contracts axially to hold its body inside the pipe and then propagates with backward contraction and expansion of the body segment. This robot is easy to downsize and has a flexible structure, but its traveling speed is slow; therefore, the time required for inspection is considerable. The traction force is large because it is actively generated by air pressure. However, the propulsion force is small because it is passively generated by the restoring force of the robot's body. Therefore, the contracted body segment cannot be restored in complex pipes, and the estimation of the propulsion speed and propagating through the pipes become difficult [9], [10].

However, when the inchworm-type travels inside the pipelines, its posterior body segment-first expands in the radial direction to hold it inside the pipe. In this state, the front body segment is extended first. This expansion and extension enable the forward propagation of the robot. Moreover, the robot is easier to downsize, has a more flexible structure, travels faster, and has a larger propulsion force than the earthworm-type robot. Therefore, it can travel in complex pipelines within a short period. However, the traction force is small because it is passively generated by the restoring force of the robot's body. Therefore, the extended body segment of this robot cannot be restored in long pipes. Furthermore, the estimation of traveling speed and traveling itself becomes difficult [11], [13]. Additionally, as these robots travel intermittently, owing to the wave propagation of the elastic passive elements, the traveling distance in long or complex pipes decreases significantly. In this manner, the traveling speed of fluid-driven robots is affected by pipe influences, which in turn hinders planned pipeline inspections [13]. Therefore, it is desirable to actively generate both the propulsion and traction forces in a robot-driven manner by generating intermittent longitudinal waves using fluid pressure. However, actuators must be added to actively generate both of these forces. Consequently, the tube for driving the actuators in the limited areas inside the pipes must be doubled.

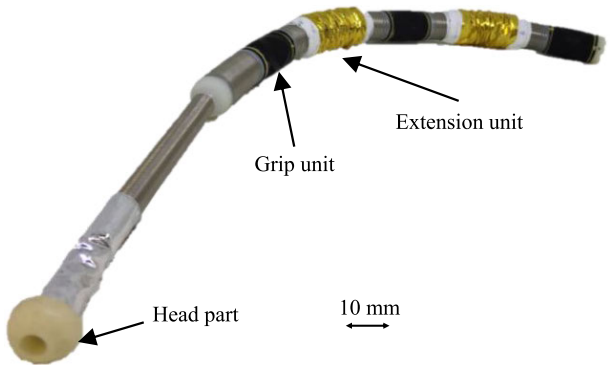

FIGURE 1. Flexible PI-RO (Pipe Inspection RObot) that generates active propulsion and traction force.

Therefore, in this study, we developed a PI-RO, as shown in Fig. 1, capable of actively generating both the necessary propulsion and traction forces. The PI-RO is equipped with a linear antagonistic mechanism (LAM-ETF) that can actively generate both propulsion and traction forces and enhance the traction force. The PI-RO driven by wave propagation can actively generate both the aforementioned forces using the same number of actuators as conventional robots [13]. Consequently, the same amount of restoration can be achieved as designed by intermittent longitudinal waves, and the inspection speed can be estimated with superior accuracy. Therefore, using PI-RO, planned pipeline inspections can be conducted effectively. In addition, our proposed robot has a small flexible structure and is compatible with bending pipes, such as elbow pipes (90° bending pipes) often present in household piping.

In a previous study, a prototype of a PI-RO and its basic characteristics were analyzed [18]. However, in the study, the head part of the PI-RO buckled, and the buckling absorbed the force of the actuator. As a result, the propulsive force of the entire PI-RO, which is indispensable for entering the pipe, was insufficient. Furthermore, in previous studies, only the basic characteristics of the PI-RO were analyzed, and no experiments were conducted to evaluate the inspection performance in long-distance, complex thin pipes. Therefore, the feasibility of inspection with PI-RO incorporating LAM-ETF in long-distance, complex small-diameter pipes, such as gas pipes, was not determined.

Therefore, the purpose of this study is to evaluate the effectiveness of PI-RO for gas pipe inspection. To counter the decrease in the propulsive force due to buckling of the PI-RO in the previous study, the joint of the PI-RO was changed to a tension spring capable of transmitting propulsive force, and the characteristics of the PI-RO were analyzed. Furthermore, inspection experiments were conducted on long-distance complex pipelines. The characteristics of the proposed LAM-ETF were estimated first. Furthermore, after verifying the movement characteristics of the PI-RO in the pipe (propulsion and traction force), its traveling and inspection performance was evaluated by conducting experiments on long and complex pipelines.

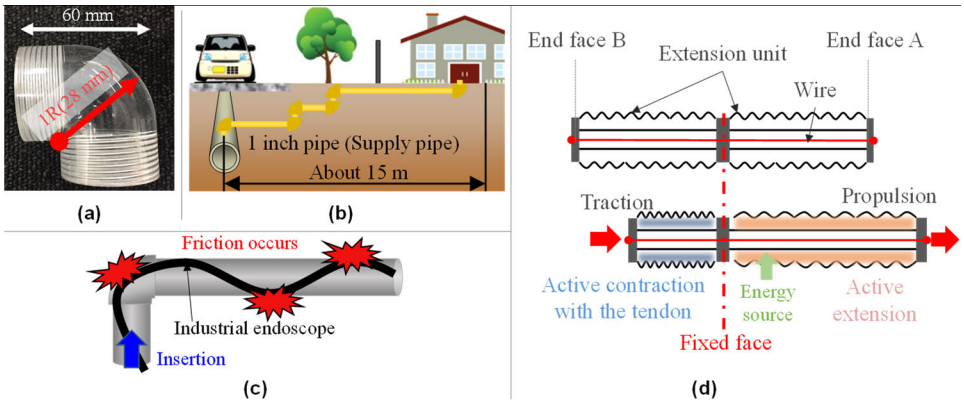

FIGURE 2. Gas pipe installation method, issues in its inspection, and the working principle of this study. (a) is the elbow pipe (90° bending pipe); the material of this pipe is acrylic, and the inner side is transparent. The actual material used is iron. (b) shows installation examples of household pipes. Pipes connect the household to the supply source. (c) shows the endoscope in a bending pipe. When friction occurs between the endoscope and the inner wall of the pipe, the endoscope bends, and the inspection of the entire pipe becomes difficult. (d) shows the working principle of an active output mechanism that enables the active generation of both propulsion and traction forces.

The contributions of this study are as follows.

- To achieve gas pipe inspection, a method of antagonistically driving actuators, which enhances both traction and propulsion forces in a narrow pipe, was developed.
- The performance of the developed robot was evaluated by inspection tests in a pipeline similar to the actual working environment.
- The advantages and disadvantages of the proposed driving method were verified by comparing it with the existing driving methods.

II. CURRENT STATUS OF HOUSEHOLD PIPING INSPECTION

A. INSTALLATION STATUS OF HOUSEHOLD PIPES

The target household pipe used in this study was hard (material: iron), one inch thick (inner diameter: approximately 28 mm), with a standard length of approximately 15 m. This pipe had an elbow, as depicted in Fig. 2 (a), with a curvature radius of 28 mm and a 90° bend. There were multiple sharp bends in the pipeline. Fig. 2 (b) shows an example of a piping installation. Household pipelines are used to connect water and gas supply sources to each household. The long-term use of these household pipes results in cracks and corrosion. Such deterioration not only hinders the stable supply of water and gas but may even lead to hazardous events, such as explosions caused by gas leakage. Thus, to prevent such problems, frequent inspection of household pipes is necessary.

B. HOUSEHOLD PIPE INSPECTION METHOD AND PROBLEMS

Common inspection techniques include disassembly and nondestructive inspection techniques. In the former, the pipe is disassembled and inspected only once, followed by its reassembling and restoration. This method is extremely time-consuming. In contrast, in the latter, the operator pushes an industrial endoscope into the pipe, which causes the wire to buckle. However, when the endoscope is pulled out from the pipe, the pulling force of the operator is transmitted to the entire wiring, and the endoscope does not buckle. However, when pushing the endoscope, the force of the operator is not sufficiently transmitted to the tip of the endoscope, as shown in Fig. 2 (c). Therefore, it becomes difficult to push the endoscope into the pipes, and inspecting complex and long pipelines become difficult.

Furthermore, considering the current usage of household pipes, the entire pipeline must be inspected within an hour. Therefore, it is necessary to develop a self-propelled endoscope that can inspect complex and long pipes, without the aforementioned issues.

C. REQUIRED PERFORMANCE OF THE HOUSEHOLD PIPE INSPECTION ROBOT (PI-RO)

In the nondestructive inspection of household pipes, the robot has to move approximately 30 m back and forth in the pipe, as shown in Fig. 2 (b). As these pipelines are constructed in a three-dimensional manner (vertically and horizontally), long-distance and multiple elbow pipes need to be traversed during the inspection. Therefore, we have developed a mobile robot capable of inspecting complex, long, and narrow pipelines with multiple elbow pipes.

D. CHALLENGES OF EARTHWORM AND INCHWORM TYPE ROBOTS

The earthworm-type robot traverses a long-distance pipe by actively exerting large traction forces, generated using fluid pressure, but the propulsion force depends on the elasticity of the material of the robot. Therefore, the propulsion force can be increased by increasing the elasticity of the material. However, the earthworm-type robot is inflexible, and therefore, the propulsion performance in the bending pipe is significantly impaired.

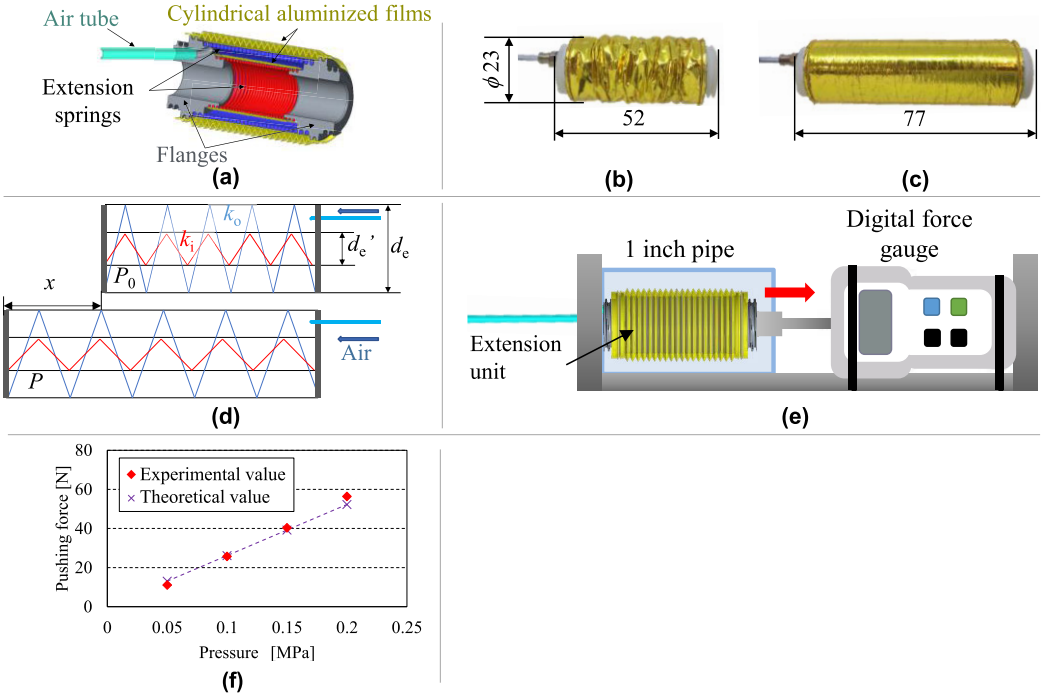

FIGURE 3. The structure and characteristics of LAM-ETF. (a) is the Internal structure of the extension unit. (b) and (c) are the appearances of the extension unit. (b) is the decompressed state, and (c) is the pressurized state. (d) is a force model of LAM-ETF. The propulsion and traction of the LAM-ETF were estimated from a model of the generated force of a single extension unit. (e) shows the environment for measuring the pushing force of an extension unit. (f) shows the results of the pushing force of an extension unit. The theoretical value in the case of the generated force in the natural length state of the extension unit calculated from Eq. (1) is also described in (f). There is no effect of the internal springs on the pushing force of the extension unit because the springs are of natural length.

In contrast, the inchworm-type robot actively generates the propulsion force using fluid pressure. Inchworm robots can, therefore, penetrate complex pipes, but their traction depends on the elasticity of the material. Consequently, inchworm robots are generally unable to traverse long-distance pipelines.

The traveling speed of robots such as earthworms- or inchworm-type robots, with elastic passive elements, is significantly affected by the surrounding environment. Thus, moving forward while inspecting a long-distance complex pipe as well as the estimation of the traveling speed becomes challenging; therefore, such robots are unsuitable for planned pipe inspections. Therefore, a robot that can actively generate both propulsion and traction forces must be developed; however, in such a robot, the number of air tubes to be pulled increases. Multiple air tubes are difficult to pull owing to the limited physical space inside the pipelines. Therefore, a new method to address these problems is required.

III. LINEAR ANTAGONISTIC MECHANISM FOR ENHANCING TRACTION FORCE (LAM-ETF)

A. CONCEPT OF LAM-ETF

To address the problems associated with earthworm- and inchworm-type robots in the limited space inside pipelines, we propose a mechanism, as shown in Fig. 2 (d). The proposed mechanism, called LAM-ETF, is capable of actively generating both propulsion and traction forces.

TABLE 1. Specifications of extension spring of extension unit.

	Length [mm]	Outer diameter [mm]	Wire diameter [mm]	Material
Outer spring	25	20	1.2	SUS304W P-B
Inner spring	20.8	14	0.8	SUS304W P-B

The LAM-ETF comprises two linear antagonistic units, which utilize tendons. These units actively extend by supplying an energy source. In this study, an air source was used as the energy source. These units are referred to as extension units.

When the extension unit on the right side extends, a force is generated to the right of the end face A. The end face B is simultaneously pulled in by the tendon, which is connected to both the end faces. By transmitting the force generated, it is possible to actively generate both pushing and pulling forces. As this mechanism is symmetrical, the operation can be reversed when driving the extension unit in the opposite direction.

B. THEORETICAL PROPULSION AND TRACTION FORCE OF THE LAM-ETF

The extension units were constructed as air pressure driven. The structure of the extension unit is illustrated in Fig. 3 (a). When air pressure was applied between the two cylindrical

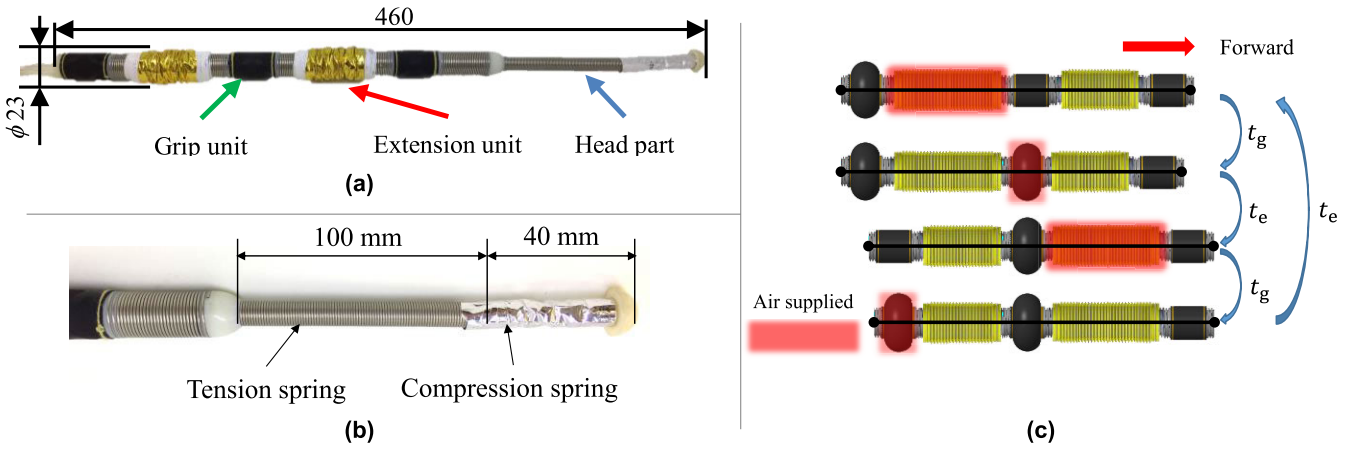

FIGURE 4. Outline of PI-RO. (a) is the appearance of PI-RO. (b) is the operation pattern of each unit of the PI-RO. (c) is the head parts of the PI-RO.

TABLE 2. Specifications of PI-RO.

Length [mm]	Maximum outer diameter [mm]	Mass [g]	Number of units [-]	Number of units [-]
460	23	150	5	5

TABLE 3. Dimensions of spring used for the head part.

	Outer diameter [mm]	Inner diameter [mm]
Compression spring	10.0	8.0
Extension spring	8.4	6.0

aluminized films of the extension unit, the pressure was applied axially to the flange. The air pressure acting on this flange extended the extension unit. When the application of pressure was stopped, the air was exhausted, and the elastic force of the extension spring returned to its initial state (Fig. 3 (b) and (c)). The spring inside the extension unit exerted a rotational force when it was extended. On the other hand, the outer film of the extension unit extended while exerting a force to cancel the rotation, as shown in Fig. 3 (c). However, the rotational force was thought to be too small because the active coils of the springs used for the extension units were large compared to the length of the extension. The inner extension spring prevents the film from being pushed inward by the air pressure, whereas the outer extension spring prevents it from being caught in the steps inside the pipe. The extension unit had a hollow structure, which allowed the tendons and air tubes to pass through easily.

As depicted in Fig. 3 (d), the force of the LAM-ETF was estimated using the force model of an extension unit. The outer diameter of the extension unit is d_e, inner diameter is d_e', applied air pressure is P, spring constant of the outer extension spring is k_0, spring constant of the inner extension spring is k_i, the natural length of the extension unit is x_0, and the length of the extension unit is x_e. Considering the restraint on the amount of elongation by the sheet (aluminized film in this study), the maximum length of the extension unit is x_{max}, and the theoretical pushing force F_{th} of the extension unit is given by Eq. (1). The pushing force, expressed by Eq. (1), can be converted into propulsion and traction forces.

$$F_{th} = \begin{cases} \pi P(d_e^2 - d_e'^2)/4 - (k_o + k_i)(x_e - x_0) & (x_e < x_{max}) \\ 0 & (x_e \geq x_{max}) \end{cases} \quad (1)$$

C. PROTOTYPE AND STRUCTURE OF THE LAM-ETF

As the propulsion and traction forces of the LAM-ETF depend on the force exerted by the extension unit, it should have a higher and better output. Considering that the force exerted by the extension unit is directly proportional to the pressure receiving area and the clearance area within the pipe's inner wall, the outer diameter of the extension unit d_e was set to 23 mm, such that approximately 80% of the cross-sectional area of the pipe was equal to that of the extension unit. The inner diameter of the extension unit was set to 11 mm, considering the space through which the tendon passes. Table 1 lists the specifications of the extension spring. In addition, an effective spring was selected as the extension spring of the extension unit by considering the unit dimensions.

Fig. 3 (b) and (c) illustrate the appearance of the developed extension unit. A folded aluminum film was used as the bellow. The extension unit was extended when the air pressure applied was approximately 25 mm.

D. GENERATING FORCE OF THE LAM-ETF

In this section, to verify that the maximum force concerning the pressure required for long-distance inspection was by the proposed model, we measured the pushing force along with the air pressure. Here, the pushing force of the extension unit is converted into propulsion and traction forces by the LAM-ETF. Therefore, the changes in the pressure applied to the extension unit were measured, and the propulsion and traction forces generated were estimated using the LAM-ETF.

Fig. 3 (e) shows the experimental environment for measuring the pushing force of the extension unit. First, the extension unit was fixed to a wall. Next, a digital force gauge was fixed at a position from the wall where the extension unit had a

natural length. In this state, air pressure was applied to the extension unit, and the pushing force of the extension unit was measured using the digital force gauge.

During a pressure resistance test conducted on the prototype unit in advance, the pressure that could be applied without bursting the extension unit was 0.30–0.40 MPa. Therefore, in this paper, 0.20 MPa is set as the upper limit pressure so that the unit can be driven stably without bursting during the experiment.

The pressure was applied in steps of 0.05 MPa between 0.05 MPa and 0.20 MPa, and the average indentation force was obtained from five measurements under each pressure condition. Furthermore, the extension unit was composed of a spring, and the hysteresis was small. Therefore, it is possible to verify the tendency of the force that is exerted by the extension unit from the experimental results and Eq. (1).

Fig. 3 (f) shows the pushing-force measurement results of the extension unit. This result also describes the theoretical indentation force obtained using Eq. (1). Here, this theoretical value shows the force in the natural length state, and it is evident that the spring had a negligible effect on the extension force. From this result, it can be inferred that the pushing force increases linearly with an increase in the applied pressure. The pushing force was 56.4 N for air pressure of 0.20 MPa, which was the maximum pressure applied in this case. The results were found to be in agreement with the theoretical values from Eq. (1). However, in some cases, the measured values exceeded the theoretical values. The pushing force of the extension unit is affected by the square of the bellow diameter obtained from Eq. (1). Therefore, it can be concluded that the dimensional error of the two handmade bellows used in the extension unit had a significant impact on the output forces generated.

IV. OUTLINE OF PI-RO WITH LAM-ETF

A. PI-RO

Fig. 4 (a) shows the external appearance of the PI-RO equipped with the LAM-ETF, and Table 2 details the specifications of the PI-RO. First, the gripping unit was mounted in the center because the force generated by the extension unit was transmitted by the linear antagonistic drive mechanism. In addition, the front and rear gripping units were configured to keep front and rear movements the same. During the symmetrical movements and intrusion into the pipe, PI-RO moves out of the pipe. Based on this concept, we designed a robot with a minimum number of units.

As shown in Fig. 4 (a), the proposed PI-RO had a head part, three grip units, and the LAM-ETF extension unit connected via extension springs. The grip units were arranged at the front, rear, and center of the extension unit. The air tubes and tendons for driving each unit were installed inside the PI-RO.

Fig. 4 (c) shows the operation pattern of PI-RO. First, the PI-RO was secured in a pipe with the rear grip unit. Next, the extension unit was extended, and the PI-RO was propelled. Thereafter, the PI-RO was fixed again utilizing the front gripping unit. This motion then propagated from the rear to the front of the PI-RO, which then traveled forward. As the PI-RO was equipped with the LAM-ETF extension unit, the tendon that constrained the entire length of the PI-RO transmitted the extension force of one extension unit to the other and forced the other extension unit to contract. In this way, the pushing force of the extension unit was dispersed into the propulsion and traction forces; thus, it became possible to generate both active outputs. The PI-RO can travel in a vertical pipe by inflating at least one grip unit and fixing the PI-RO in the pipe itself. As the PI-RO has a symmetrical structure, the direction of propagation can be reversed by reversing the operation pattern.

It is difficult to push the endoscope into pipes. However, it is easy to pull out the endoscope from a pipe because the pulling force of the operator can be transmitted to the entire wiring.

Therefore, the purpose of this study was to realize the towing of wiring into a pipe with a self-propelled robot. To pull the endoscope out from complex pipes, the diameter of the PI-RO must be smoothly changed so that the PI-RO would not get caught in the elbow of the pipe. Therefore, the entire circumference of the PI-RO was tapered to prevent it from getting caught on the steps of the pipe.

Taking the operation pattern into consideration and the load to tow the wiring, the theoretical speed can be evaluated using Eq. (2) and (3), assuming that the displacements of the grip unit and operating time are x_g and t_g, respectively, the natural length of the extension unit is x_0, the length of the extension unit and operating time are x_e and t_e, respectively, and the force for traction is F_{tra}. X_P is the pressure threshold for the maximum length of the extension unit. According to Eq. (3), the PI-RO inspection speed decreases owing to the load F_{tra}.

$$V_{th} = \left[(x_e - x_0) + x_g\right] / 2(t_g + t_e) \tag{2}$$

$$x_e = \begin{cases} x_0 + \dfrac{\frac{\pi P(d_e^2 - d_e'^2)}{4} - F_{tra}}{(k_0 + k_i)} & (P < X_P) \\ x_{max} & (P \geq X_P) \end{cases}$$

$$X_P = \frac{4\,(k_0 + k_i)\,(x_{max} - x_0) + F_{tra}}{\pi(d_e^2 - d_e'^2)} \tag{3}$$

B. STRUCTURE AND SPECIFICATIONS OF HEAD PART

Fig. 4 (b) illustrates the appearance of the head part, and Table 3 details its specifications. The head part was composed of an extension spring, a compression spring, and a hemispherical acrylonitrile-butadiene-styrene (ABS) plastic resin. The hemispherical ABS resin was connected to the leading unit by extension and compression springs. The head part was hollow so that the wiring of the camera and sensor could pass through it. The head part could be flexibly bent in the bending tube by the compression spring connected to the ABS plastic parts, thereby enabling deformation and propulsion of the robot according to the shape of the tube. The compression spring deforms and propels along the pipe, which allows the

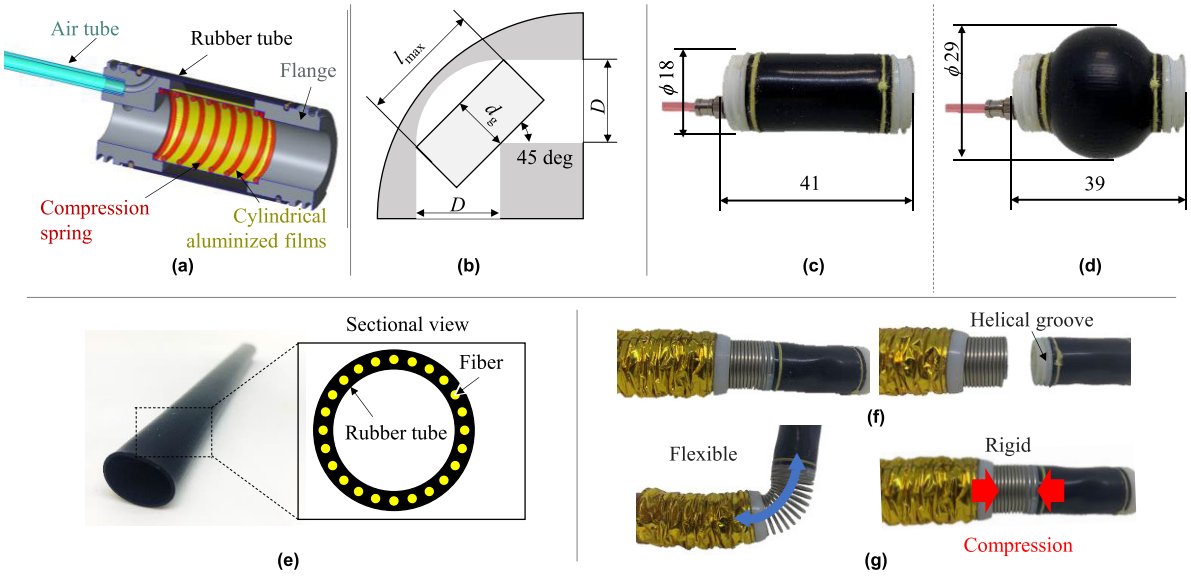

FIGURE 5. The concept and design of the grip unit and joint unit. (a) is the internal structure of the grip unit. (b) is the elbow pipe passage model of the grip unit. (c) and (b) is the appearance of the grip unit. (c) is the decompressed state, and (d) is the pressurized state. (e) is the appearance of the straight fiber type rubber tube. (f) and (g) are joint connection methods and their behavior. (f) shows the appearance and installation method of the joint part. Each unit can be connected by screwing the joint part into the groove of each unit. (g) shows the features of the extension spring joint part. The left image shows the flexibility when passing through a curved pipe. The right shows the high pushing force transmission performance.

TABLE 4. Specifications of the spring used for grip unit.

Length [mm]	Outer diameter [mm]	Wire diameter [mm]	Material [-]
20	13	1.0	SWP-A

TABLE 5. Specifications of the flexible joint part.

Length [mm]	Outer diameter [mm]	Wire diameter [mm]	Material [-]
15.6	18	1.2	SUS304WP-B

entire PI-RO to pass through an elbow pipe. In the head part, the circumference of the compression spring was covered with an aluminized film so that the groove existing between the pitches of the compression spring was not caught up in the step inside the pipe.

C. STRUCTURE AND SPECIFICATIONS OF THE GRIP UNIT

Fig. 5 (a) shows the structure of the grip unit. Air flowed into the chamber between the rubber tube and the film when air pressure was applied to the grip unit. With the inflow of air, the grip unit expanded radially and contracted axially, as shown in Fig. 5 (c) and (d). The grip unit fixed the PI-RO in the pipe by radial expansion owing to the application of air pressure. When the air was exhausted, the grip unit returned to its initial state owing to the elastic force of the rubber tube and compression spring, and the PI-RO was released. As the grip unit was hollow, it could easily pass through the tube. The surface of the gripping unit was designed to be as smooth as possible to prevent it from being caught in the step.

Fig. 5 (b) shows the elbow pipe passage model of the grip unit. The outer diameter of the grip unit d_g was set to 18 mm, considering the inner pipe diameter (D = 28 mm), cross-sectional area of the air tube, tendon passing through the unit and the wall thickness of the flange. In this study, the maximum length of the grip unit was l_{max} = 43.1 mm from (4). Therefore, the length of the grip unit was set to 41 mm.

$$l_{max} = 2(\sqrt{2}\,D - d_g) \tag{4}$$

Fig. 5 (c) and (d) show the appearance of the developed grip unit. The straight fiber-type rubber tube is shown in Fig. 5 (e) [19]. The outer diameter of the grip unit was approximately 29 mm when the air pressure was applied, and the grip expanded more than the inner diameter of the pipe. Table 4 lists the specifications of the compression spring, which is a component of the grip unit. The compression spring has a significant influence on the rigidity of the gripping unit and is related to the elbow pipe passage performance. Therefore, an effective spring was selected as the compression spring of this gripping unit for passage through a bending pipe, considering the limitations due to the dimensions. In addition, to pull the PI-RO out from the complex pipes, the diameter of PI-RO was smoothly changed so that the PI-RO would not get caught in the elbow of the pipe.

It was assumed that there was no water accumulation at the time of inspection because the target pipes in this study carried gas, and there were no significant changes in the frictional force of the gripping unit. In addition, by increasing the applied pressure of the artificial muscle, it was expected that the gripping force would increase. Furthermore, it was assumed that the expansion diameter could be changed in response to a slight change in the pipe diameter because the gripping unit had a flexible gripping structure.

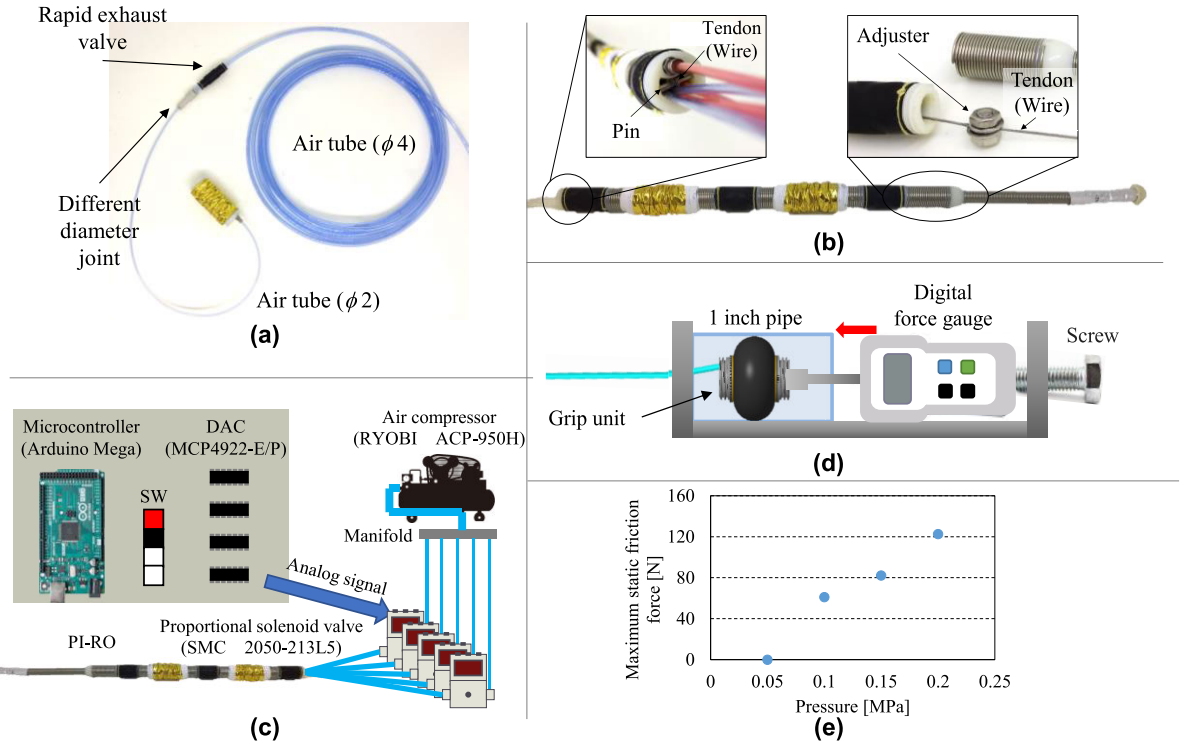

FIGURE 6. PI-RO components, characteristics, and actual LAM-ETF. (a) shows the methods for connecting air tubes and the devices that supply air and improve the exhaust speed of each unit. (b) shows the tendon attachment position and attachment method in the LAM-ETF. (c) shows the operating system of the PI-RO. The air pressure inside each unit can be operated independently of the system. (d) is the gripping force measurement environment of the grip unit. (e) is the gripping force measurement result of the grip unit.

D. STRUCTURE AND SPECIFICATIONS OF THE JOINT PART

Fig. 5 (f) illustrates the joint part that connects each unit of the PI-RO, and Table 5 details its specifications. A groove was spirally formed on the flange of each unit, and each unit was connected by a screw in the joint part. This joint part had features that enabled the units to be firmly connected and to be easily attached and detached. As this part is flexible, it can be curved along a bending pipe, as shown in Fig. 5 (g). When receiving the force generated from the extension unit, it behaves as a rigid body in the axial direction and reliably transmits the force forward, as shown in Fig. 5 (g).

The PI-RO was passively bent by the pushing and pulling forces of the proposed mechanism. The pushing force of the extension unit pushed the PI-RO forward. In addition, the rearmost unit of the PI-RO was pushed in the propulsion direction by the force transmitted by the proposed mechanism. This pushing force caused the PI-RO to passively bend owing to the reaction force from the inner wall of the bending pipe. Therefore, the robot bent flexibly along the shape of the pipe and could pass through the elbow pipes.

E. TUBES FOR SUPPLYING AIR PRESSURE

Each unit was driven pneumatically. Therefore, it was necessary to connect an air tube to each unit. There was a plan to connect the air tubes into spiral shapes. However, the cross-sectional area inside the PI-RO was small, and it was difficult to mount multiple spiral air tubes. Therefore, the air tubes were designed with a margin in length and did not interfere with the crawling of the PI-RO. When a PI-RO is inspected, the air tubes inside the robot slide. To apply air pressure to each unit, an air tube (SMC, TU0212BU-20) with a length of 0.4 m and an inner diameter of 1 mm was connected, as shown in Fig. 6 (a). Using a joint with different diameters (SMC, KQ2H02-04A), an air tube with a length of 15 m and an inner diameter of 4 mm (PISCO, UBT0425-20-CB) was connected to the air tube mentioned earlier.

F. INSTALLATION METHOD OF THE LAM-ETF

Fig. 6 (b) shows the fixed end of the tendon. The tendon was fixed to the grip unit at the front and rear ends of the PI-RO. The tendon length at the front end was varied using an adjuster. The tendon length and diameter were 298 mm and 1 mm, respectively. This tendon length was the shortest and could be fully extended by the extension unit used for the LAM-ETF. In addition, a rapid exhaust valve (PISCO, EQU-4) was installed at the same location as the air tubes at different diameter joints to accelerate the exhaust response in each unit.

G. OPERATING SYSTEM OF THE PI-RO

Fig. 6 (c) shows the operating system of the PI-RO. It comprises a microcontroller (Arduino Mega), DAC (MCP4922-E/P), compressor (RYOBI, ACP-950H), manifold, proportional solenoid valve (SMC, 2050-213L5), and

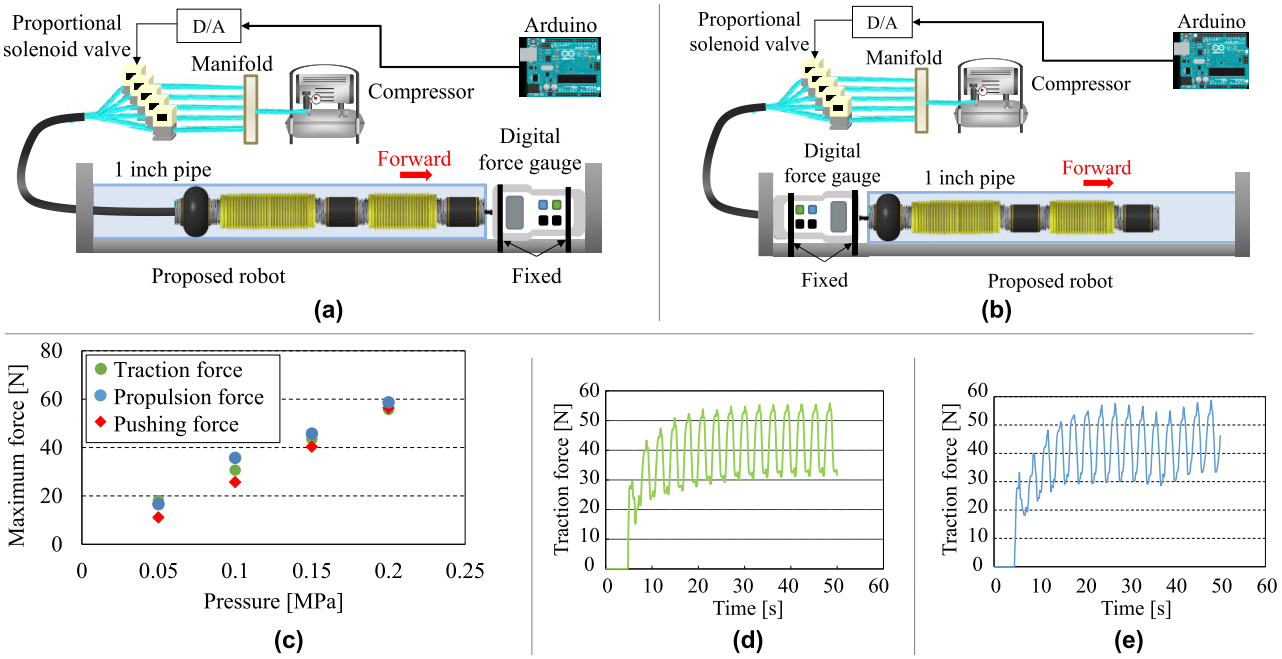

FIGURE 7. PI-RO propulsion and traction force measurement experiment environment and results. (a) is the propulsion force measurement experiment. (b) is the traction force measurement experiment. (c) is the comparison of the maximum propulsion and traction forces. The force generated by the extension unit (pushing force) is shown. (d) and (e) are the time response waveforms of propulsion and traction. (d) is the traction force waveform when 0.20 MPa is applied, (e) is the propulsion force waveform when 0.20 MPa is applied. In both cases, the force increases with time and becomes a steady state.

pushbutton switches (SW). The PI-RO was passively bent in the bent pipe. Owing to the characteristics of the flexible robot (soft actuator) and flexible deformation according to the environment, complicated controls were not required for continuous in-pipe inspection without branching. Therefore, only the forward/backward movement and the stopping of the PI-RO were controlled by a manual switch. The repetitive operation assigned to the SW was the output from the microcontroller. The output digital signal was then converted to an analog signal by the DAC and fed to the proportional solenoid valve. Subsequently, the air pressure supplied from the compressor was adjusted according to the input voltage using the proportional solenoid valve and then supplied to the PI-RO. This enabled each unit to operate independently.

In this paper, we proposed a robot with a mechanism that can actively exert both propulsive force and traction force. On the other hand, the duration of the operation and the inspection speed of the PI-RO equipped with this mechanism were not optimum. In the future, we would like to improve the inspection speed concerning the response of each unit. Therefore, "Regarding the intake /exhaust response of the series antagonistic drive mechanism" was added to the prospects.

H. GRIPPING FORCE OF THE PI-RO

In this section, the air pressure characteristics (maximum static friction force) due to the changes in the pressure of the grip unit were estimated. The maximum static friction force of the grip unit determines whether the PI-RO can be fixed in the pipe. Therefore, the propulsion and traction forces that the PI-RO can output are less than the maximum static friction force of the grip unit. Based on the abovementioned considerations, the air pressure characteristics of the grip unit under pressure changes were verified based on the measured values, and the pressure required for the PI-RO to travel in the pipe was obtained.

Fig. 6 (d) depicts the experimental environment for the maximum static friction force measurement. First, a grip unit was placed in a fixed pipe (inner diameter of approximately 28 mm), and air pressure was applied. Next, the digital force gauge was slid forward with a screw and pressed against the grip unit.

Next, the force output when the grip unit slipped out was measured using a digital force gauge. The pressure was applied in steps of 0.05 MPa between 0.05 MPa and 0.20 MPa, and the average indentation force was obtained from five measurements under each pressure condition.

Fig. 6 (e) shows the measurement results for the maximum static friction force of the grip unit. This result demonstrates that the maximum static friction force increases in a nonlinear manner. This increase in force was due to the increase in the force with which the grip unit pressed the pipe wall with increasing pressure. The maximum static friction force was 122.7 N when a pressure of 0.20 MPa was applied.

Therefore, it can be inferred that the propulsion and traction forces that the PI-RO can output are 122.7 N or less when the maximum applied pressure is 0.20 MPa. However, when the applied pressure was 0.05 MPa or less, the tube wall was not gripped even when the grip unit expanded. When the entire circumference of the grip unit is not in contact with the

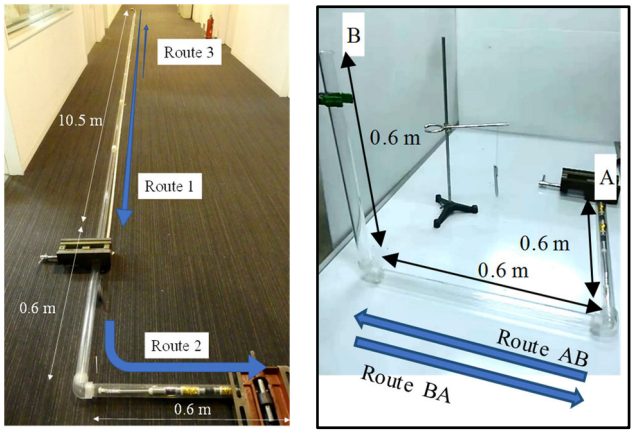

FIGURE 8. Crawling experiment environment of the PI-RO. (a) Routes for the long-distance pipe are Routes 1 to 3. (b) Routes for the multi-elbow pipe are Routes AB, BA.

pipe wall, the internal pressure does not act perpendicular to the pipe wall, and consequently, the maximum static friction force decreases.

V. PROPULSION AND TRACTION FORCE MEASUREMENT EXPERIMENT WITH LAM-ETF

A. OUTLINE OF PROPULSION AND TRACTION FORCE MEASUREMENT EXPERIMENTS

The air pressure characteristics (propulsion and traction force) of the PI-RO were measured, and the change in the output due to the pressure changes was verified. The propulsion force represents the performance of a system when passing through a curved pipe, such as an elbow pipe. Therefore, highly complex pipe inspections are possible only if large propulsion forces are generated. The traction force indicates the extent to which a towed object can be pulled into the pipe. The greater the traction force, the deeper the object is pulled into the pipe. From the measured values, the LAM-ETF converted the force generated by the extension unit into propulsion and traction forces and confirmed whether these forces could be actively output.

B. PROPULSION AND TRACTION MEASUREMENT ENVIRONMENT

Fig. 7 (a) and (b) depict the experimental environments for the propulsion and traction force measurements, respectively. The pipe and digital force gauge were fixed, and the PI-RO was made to crawl in the pipe for 50 s.

The propulsion force was measured by pressing the PI-RO directly against the digital force gauge. The traction force was measured by connecting the tendons of the PI-RO and the digital force gauge. The sampling frequency was set to 10 Hz, and a pressure of 0.20 MPa was applied to the grip unit, which was sufficient to support the maximum pushing force (56.4 N) of the extension unit. The operating times for each unit are listed in Table 6.

TABLE 6. Time for measuring PI-RO propulsion and traction.

	Grip unit	Extension unit
Operation time [s]	0.42	0.80

TABLE 7. Operating time for measuring PI-RO crawling experiment.

	Grip	Extension unit
Applied pressure [MPa]	0.2	0.2
Operation time[s]	0.20 (t_g)	0.80 (t_e)
Displacement [mm]	2 (x_g)	25 (x_e)

C. RESULTS AND DISCUSSION OF PROPULSION AND TRACTION FORCE MEASUREMENT EXPERIMENTS

Fig. 7 (c) shows a graph summarizing the maximum values of the propulsion and traction forces under each applied pressure. In addition, Fig. 7 (d) and (e) show the waveforms of the propulsion and traction forces, respectively, when a pressure of 0.20 MPa was applied. The figures show that the waveform tendencies at each applied pressure were the same. From Fig. 7 (d) and (e), it can be inferred that the maximum values of both the propulsion and traction forces monotonically increase with increasing pressure.

Therefore, based on the abovementioned results, it was confirmed that the LAM-ETF converts the force generated by the extension unit into propulsion and traction forces and then actively outputs them. However, the output varied slightly between the propulsion and pushing forces. The force generated by the extension unit in Eq. (1) in Section III, Section C is proportional to the receiving cross-sectional area and internal pressure. Therefore, the pressure-receiving area was dominant in the output when a low pressure was applied. As shown in Fig. 7 (c), the output difference is large when low pressure is applied and small when high pressure is applied. This output difference is due to the error in the pressure receiving area fabrication because the error increases when low pressure is applied, where the pressure receiving area is dominant.

From Fig. 7 (d) and (e), it can be inferred that the propulsion and traction forces increase over time and gradually become steady. When the PI-RO began to operate, the restoring force of the extension unit affected the output, and after a certain period, the extension unit could not be further extended. Subsequently, the propulsion and traction forces were at their maximum values.

Therefore, the forces increase with time. In addition, as the PI-RO repeats certain operations, the peaks occur when the extension unit inhales, and the forces tend to drop sharply when the gripping unit is exhausted.

VI. TRAVELING EXPERIMENT IN THE PIPE

A. OUTLINE OF THE TRAVELING EXPERIMENT IN THE PIPE

It was confirmed before beginning the crawling experiments that the PI-RO could pass through the horizontal, vertical, and elbow pipes. Therefore, in this section, we verify the traveling feasibility of the developed PI-RO in a traveling experiment

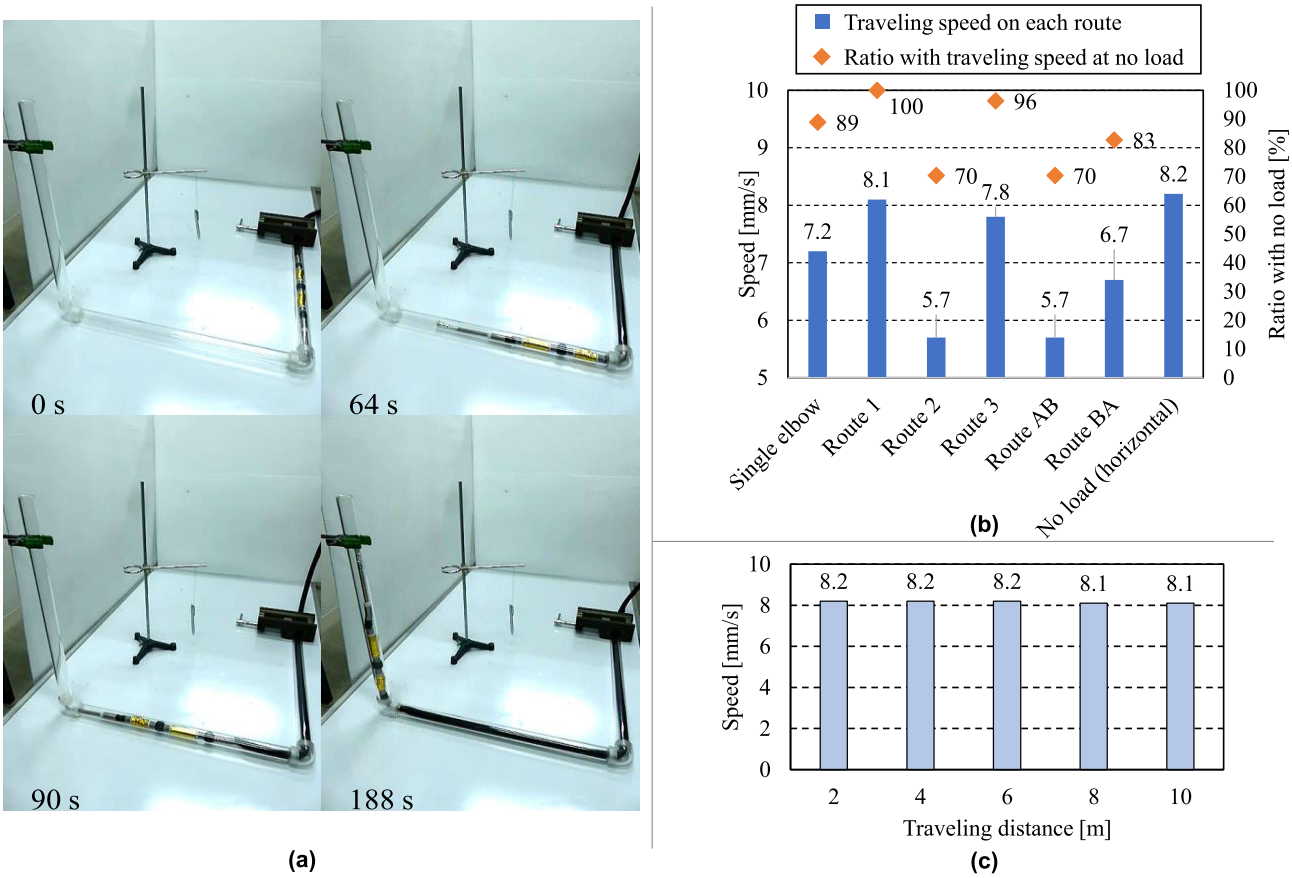

FIGURE 9. The results of the traveling experiments. (a) shows Frame-by-frame movie of PI-RO crawling on Route AB. (b) shows the comparison of traveling speed in the experiments. The traveling speed in the horizontal pipe applied in no force is also shown. (c) shows the traveling speed for every 2 m in Route 1.

in a pipeline that combines horizontal, vertical, and elbow pipes similar to an actual environment. Furthermore, a stable inspection speed for each pipe was estimated. Therefore, to verify the inspection performance of the long-distance and complex piping layouts, five piping layouts (1) Routes 1, 2, 3, and (2) Routes AB and BA were prepared. The pipelines used in this experiment were (1) long-distance pipelines and (2) multiple-elbow pipelines. In Route 1, the basic inspection performance of the PI-RO, when moving in a long-distance pipe, was verified. In Route 2, the elbow pipe passage performance of the PI-RO, when there was a load from the towed object, was verified. Furthermore, in Route 3, the long-distance inspection performance, when the towed object was inside the elbow pipe and a large load was applied to the PI-RO, was verified. In addition, in Route AB and Route BA, the inspection performance of the PI-RO for a complex small-diameter pipe, when the direction of gravity was different, was verified. As these pipes were long or had multiple elbow pipes, the propulsion and traction forces required for traveling within the pipes were large.

In addition, the pipe environment may affect the traveling speed. In the environment described above, the load acting on the conventional fluid-driven robot that generates the propulsion or traction force only by the rigidity of the material has a significant influence on the moving speed. Therefore, the theoretical speed is significantly different from the actual speed. The PI-RO, which can actively generate the propulsion and traction force, is expected to have a theoretical speed that is in agreement with the actual speed by obtaining a certain amount of displacement. A comparison of the theoretical and actual speeds based on the abovementioned considerations is one of the objectives of this experiment. From the results, it was confirmed that the PI-RO can reliably obtain the displacement amount by providing active output.

B. CRAWLING ENVIRONMENT

Fig. 8 (a) and (b) depict the experimental environment for long-distance pipe crawling and multiple-elbow pipe crawling experiments, respectively. In the long-distance pipe crawling experiment, the PI-RO was made to crawl in a pipe with a total length of approximately 12 m, including an elbow pipe. The tube was fixed to the floor with a vise so that it was horizontal to the ground.

A traveling experiment was conducted using the pipelines mentioned above along the routes shown below. In the multiple-elbow pipe crawling experiment, the PI-RO crawled in the pipes, including horizontal and vertical pipes connected by the elbow pipes.

(a) Long-distance pipe crawling experiment

Route 1: Traveled 10 m in a straight pipe

Route 2: After traveling 10 m in a straight pipe, the elbow pipe was passed.
Route 3: After passing the elbow pipe, traveled 10 m in the straight pipe.
(b) Multiple elbow pipe crawling experiments.
Route AB: Traveled from A to B shown in Fig. 8 (b).
Route BA: Traveled from B to A shown in Fig. 8 (b).

A video camera was used to capture the appearance of the crawling PI-RO in all the experiments. The applied pressures and operating times of each unit are listed in Table 7.

C. RESULTS OF TRAVELING EXPERIMENTS AND CONSIDERATION

The PI-RO completed all routes, including long-distance pipes and multiple elbow pipes.

First, after traveling for 10 m in Route 1, the extension unit was fully extended when the PI-RO was crawling. The traction force of the PI-RO was sufficiently larger than the force required to pull the air tube.

Next, considering Routes 2 and 3, the PI-RO succeeded in passing through the elbow pipe even when the 10 m air tube was pulled. From the abovementioned results, it can be inferred that the propulsion and traction forces were actively generated, and the PI-RO passed the elbow pipe bent at 90° while pulling the tube for a long distance.

Next, considering routes AB and BA, the PI-RO crawled in a complex pipe with multiple elbows while actively outputting both the propulsion and traction forces, as shown in Fig. 9 (a).

D. EVALUATION OF TRAVELING EXPERIMENT AND COMPARISON OF SPEED OF EACH TRIAL

In this section, we evaluate the results obtained from the traveling experiments and compare the traveling speeds of the routes. Fig. 9 (b) shows the average traveling speed of the routes. The theoretical speed was calculated using Eq. (2) and compared with the speed in the single-elbow passage measured in advance.

We consider a theoretical speed of 9.0 mm/s. Fig. 9 (c) depicts the moving speed for every 2 m of Route 1. As shown in Fig. 9 (c), the PI-RO crawled at a speed of 8.2 mm/s in the unloaded state (for the first 2 m), which is approximately 7.7% lower than the theoretical speed. This decrease in speed was attributed to the fact that the center axis of the PI-RO tilted from the center axis of the pipe owing to its weight. However, in a conventional robot, the actual speed was reduced by at least 33% compared to the theoretical speed [14]. From the results, it was observed that as the PI-RO actively generates propulsion and traction forces and obtains a certain amount of displacement, the theoretical and actual speeds are relatively consistent with each other and are therefore suitable for planned inspections.

Next, we considered each route in the experiment. In Route 1, the average velocity was approximately 0.9 mm/s lower than the theoretical speed. However, almost no decrease in speed was observed throughout the route, as shown in Fig. 9 (c). In addition, during the traveling experiment of Route 1, it was visually confirmed that the extension unit was completely extended to the end. From the abovementioned observations, it was concluded that the traction force generated by the PI-RO exceeded the force required for crawling in long-distance pipes. Considering that the traveling speed of the PI-RO did not significantly decrease during long-distance travel, it can be said that the PI-RO can be used for planned pipeline inspections. Comparing the traveling speed of Route 2 with that of the elbow pipe alone, a speed reduction of approximately 19% was observed. When the PI-RO passed through the elbow pipe, it bent and, consequently, the tendon sagged. This tendon sag is a disadvantage of the full pneumatic active drives. Furthermore, the PI-RO used the restoring force to pass through a single elbow pipe. Notably, a large load was generated when the PI-RO passed through the elbow pipe after traveling for a long distance, such as in Route 2. When the tendon sagged in this state, the active output was limited, and the speed was reduced even though the PI-RO used the restoring force. From this, we can say that the active traction force output is limited owing to the sag of the tendon when the PI-RO passes through the elbow pipe after traveling for long distances, such as in Route 2, and consequently, the time required by the PI-RO to pass through the elbow pipe was long. The traveling speed in Route 3 was almost identical to Route 1. Therefore, even though there was an elbow pipe near the entrance, the effect on the traveling speed of the PI-RO was insignificant for exerting active propulsion and traction forces.

Finally, on comparing the average speeds on Route AB and BA, the speed on Route BA was found to be approximately 1 mm/s faster. This difference in speed was attributed to the time required to pass through the second elbow tube. In the case of Route BA, the weight of the air tube acted in the direction of propelling the PI-RO at the entrance section. Furthermore, the gravity in the air tube was assumed to act in the direction of separating the PI-RO from the corner inside the elbow pipe, where friction occurs when passing through the elbow pipe. Therefore, the resistance of the air tube in the first elbow tube decreased, and the PI-RO traveled within a short time.

E. COMPARISON OF ROBOTS

There are a variety of articles reviewing the methods of pipe inspection [20], [21]. In contrast, we consider the wave propagation robot types such as earthworms and inchworm robots suitable for inspection of long-distance complex pipes such as gas pipes because of their small size and high traction force as mentioned in the introduction. Therefore, a comparison of the traction and propulsion force between the wave propagation type robots and PI-RO is shown in Table 8. However, both traction and propulsion forces are not indicated in some studies. Therefore, values that are not clearly shown were estimated from the data including the maximum force of the actuator for grasping the pipe and for exerting to stretch. In Table 8, the estimated values are italicized.

TABLE 8. A comparison of in-pipe wave propagation robot.

Comparison items (Inner diameter of target pipe)	This study PI-RO	[22]	[23]	[24]	[12]	[11]	[25]
(a) Evaluation indicator H_{EI} [-]	**0.935**	**0.033**	**0.112**	**Less than 0.219**	**Less than 0.347**	**0.363**	**Less than 0.496**
(b) Traction force F_T [N]	56	19	18	UNK.? (Less than F_P)	32	*56.8* **	4.5
(c) Propulsion force F_P [N]	59	14	*10**	4.7	UNK.? (Less than F_T)	15.2	UNK.? (Less than F_T)
(e) Cross sectional area of pipe $A = \pi D^2/4$ [mm^2] (Inner diameter of terget pipe D [mm])	615 (28)	2205 (53)	625 (50)	572 (27)	615 (28)	283 (19)	227 (17)
(f) Maximum Pressure P_{max} [MPa]	0.200	0.450	0.400	0.075	0.300	0.700	0.080

* The value was estimated from the maximum grasping force of the robot in the pipe.
**The value is estimated from the maximum extension force of the actuator (pneumatic piston).

Here, given that an actuator actively extended/contracted is passively contracted/extended, the passively exerted contraction/extension force is estimated to be smaller than the actively generated force. Additionally, considering the movement method of the wave-propagating robot, it can be estimated that the traction/propulsion force dependent on the passively generated force is less than the traction/propulsion force dependent on the actively generated force. In addition, the size of the pipes inspected by the robots varied, and the applied pressure was different. Therefore, the evaluation indicator was created in consideration of the situations. It was expressed as H_{EI} that the value obtained by the sum of traction force F_T and propulsion force F_P dividing by the value of multiplying the cross-sectional area A of target pipe and applied pressure P_{max} in the following equation (5). The items listed in Table 8 (a) were calculated from Eq. (5).

$$H_{EI} = \frac{F_T + F_P}{A \cdot P_{max}} \tag{5}$$

Compared with the existing robots, PI-RO has 2.57 times higher value of the evaluation indicator H_{EI}. Furthermore, PI-RO has a close value for both traction and propulsion. From the comparison, PI-Ro can actively output both propulsive and traction forces in a narrow pipe and is expected to realize planned inspection in a long and large loaded pipe.

As described above, PI-RO can actively increase both traction and propulsion forces by applying air pressure to the unit without stiffening the robot. Therefore, PI-RO is expected to be used for the inspection of long-distance and complex small-diameter pipes.

This study aimed to check the corrosion and damage in a single continuous pipe. The PI-RO was not equipped with a position detection system. However, the advantage of PI-RO is its flexible structure and its ability to deform and move along a small pipe path without complicated controls. In the future, a position detection system will be built for the PI-RO inspections if there is a need for control or identification of damaged locations. The adaptations of a position estimation system mimicking the motion of peristalsis will be investigated [26], [27]. Furthermore, we will study the construction of a system that can sense actuator damage.

VII. CONCLUSION

A. SUMMARY

In this study, we focused on the problems associated with conventional fluid-driven in-pipe mobile robots and described the pipe (inner diameter of approximately 28 mm) inspection process using the PI-RO that exhibited high output of propulsion and traction forces. The results are as follows:

- We developed a LAM-ETF comprising two linear antagonistic actively extendable units using a tendon to realize a higher output of propulsion force and traction force. We also developed a flexible pipe inspection robot (PI-RO) using the developed LAM-ETF.
- The propulsion and traction forces of the PI-RO were measured, and it was confirmed that both forces could be actively generated. A maximum propulsion force of 58.7 N and a maximum traction force of 55.8 N were recorded.
- Preliminary experiments confirmed the passage of the PI-RO through horizontal, vertical, and single-elbow pipes. In the long-distance pipe and multi-elbow pipe passage experiments, the actual inspection rate was reduced by 7.7% compared to the theoretical speed obtained by generating an active traction force even when traveling in a long-distance complex pipe where a large load is generated on the tractor, which decreases the PI-RO speed by 33%.

Based on the obtained results, it was confirmed that the proposed LAM-ETF could actively output the propulsion and traction forces and suppress the decrease in traveling speed in long-distance complex pipes. Furthermore, it is expected that by installing the proposed mechanism, a planned in-pipe inspection can be performed even for long distances (30 m).

B. FUTURE WORKS

It is assumed that the PI-RO can crawl while maintaining a constant traveling speed even during high-weight towing in long-distance pipes, thereby facilitating planned inspections. The future research directions are listed below, based on the obtained results.

- In this study, we demonstrated via laboratory experiments the possibility of performing in-pipe inspection even in long-distance complex pipes using PI-RO. Based on this result, we plan to confirm whether the PI-RO can be used for field inspections as well as when pulling high weights.
- The traveling speed did not decrease significantly during long-distance travel. However, the speed decrease was remarkable for Route 2 and AB, which had elbow pipes. It was assumed that when the PI-RO invaded the elbow pipe, the tendon used for the linear antagonistic drive mechanism became slack. The slack of the tendon can reduce traction force. Therefore, we will devise a method to reduce the speed reduction of the PI-RO. For example, we will devise a mechanism to align the tendon of the LAM-ETF with the central axis of the PI-RO.
- In this study, the robot was fabricated manually. In the future, we aim for more precise fabrication to improve pressure resistance and robustness and to conduct further long-distance complex pipe inspections. The grip and extension units were not tested for wear or longevity. The artificial muscles used in the grip unit were used in longevity tests [19]. Therefore, we will conduct endurance tests on the grip and extension units.

REFERENCES

[1] *IPLEX R Series*, Olympus Corp., Tokyo, Japan. Accessed: Sep. 24, 2021. [Online]. Available: http://www.olympus-ims.com/ja/rvi-products/iplex-rx/
[2] S. Yoda, Y. Wakibe, and Y. Imagawa, "Inspection methods of piping," *Bull. Soc. Sea Water Sci.*, vol. 68, no. 2, pp. 57–62, Sep. 2014.
[3] P. Li, S. Ma, B. Li, and Y. Wang, "Development of an adaptive mobile robot for in-pipe inspection task," in *Proc. Int. Conf. Mechtron. Autom.*, Harbin, China, Aug. 2007, pp. 3622–3627.
[4] A. H. Heidari, M. Mehrandezh, R. Paranjape, and H. Najjaran, "Dynamic analysis and human analogous control of a pipe crawling robot," in *Proc. IEEE/RSJ Int. Conf. Intell. Robots Syst.*, St. Louis, MO, USA, Oct. 2009, pp. 733–740.
[5] A. Kuwada, K. Tsujino, K. Suzumori, and T. Kanda, "Intelligent actuators realizing snake-like small robot for pipe inspection," in *Proc. IEEE Int. Symp. MicroNanoMechatronics Hum. Sci.*, Nagoya, Japan, Nov. 2006, pp. 2006–2011.
[6] J. Liu, Y. Tong, and J. Liu, "Review of snake robots in constrained environments," *Robot. Auto. Syst.*, vol. 141, Jul. 2021, Art. no. 103785.
[7] K. Isaki, A. Niitsuma, M. Konyo, F. Takemura, and S. Tadokoro, "Development of an active flexible cable by ciliary vibration drive for scope camera," in *Proc. IEEE/RSJ Int. Conf. Intell. Robots Syst.*, Beijing, China, Oct. 2006, pp. 3946–3951.
[8] T. Takayama, H. Takeshima, T. Hori, and T. Omata, "A twisted bundled tube locomotive device proposed for in-pipe mobile robot," *IEEE/ASME Trans. Mechatronics*, vol. 20, no. 6, pp. 2915–2923, Dec. 2015.
[9] M. Takahashi, I. Hayashi, N. Iwatsuki, K. Suzumori, and N. Ohki, "The development of an in-pipe microrobot applying the motion of an earthworm," in *Proc. 5th Int. Symp. Micro Mechatronics Hum. Sci.*, Nagoya, Japan, Oct. 1994, pp. 35–40.
[10] M. Ikeuchi, T. Nakamura, and D. Matsubara, "Development of an in-pipe inspection robot for narrow pipes and elbows using pneumatic artificial muscles," in *Proc. IEEE/RSJ Int. Conf. Intell. Robots Syst.*, Vilamoura, Portugal, Oct. 2012, pp. 926–931.
[11] J. Qiao, J. Shang, and A. Goldenberg, "Development of inchworm in-pipe robot based on self-locking mechanism," *IEEE/ASME Trans. Mechatronics*, vol. 18, no. 2, pp. 799–806, Apr. 2013.
[12] K. Nomura, M. Sato, H. Takeuchi, K. Minoru, T. Ryoichi, H. Ishii, and A. Takanishi, "Development of in-pipe robot with extension hose and balloons," in *Proc. IEEE Int. Conf. Mechatronics Autom. (ICMA)*, Takamatsu, Japan, Aug. 2017, pp. 1481–1486.
[13] M. Kamata, S. Yamazaki, Y. Tanise, Y. Yamada, and T. Nakamura, "Morphological change in peristaltic crawling motion of a narrow pipe inspection robot inspired by earthworm's locomotion," *Adv. Robot.*, vol. 32, no. 7, pp. 386–397, Jan. 2018.
[14] L. Wang, T. Akagi, S. Dohta, and T. Kawasaki, "Development of slide type inspection robot using flexible pneumatic cylinder," in *Proc. Int. Conf. Adv. Mechatronics Syst.*, Tokyo, Japan, Sep. 2012, pp. 75–80.
[15] J. Min, Y. D. Setiawan, P. S. Pratama, S. B. Kim, and H. K. Kim, "Development and controller design of wheeled-type pipe inspection robot," in *Proc. Int. Conf. Adv. Comput., Commun. Informat. (ICACCI)*, New Delhi, India, Sep. 2014, pp. 789–795.
[16] S. A. Fjerdingen, P. Liljeback, and A. A. Transeth, "A snake-like robot for internal inspection of complex pipe structures (PIKo)," in *Proc. IEEE/RSJ Int. Conf. Intell. Robots Syst.*, St. Louis, MO, USA, Oct. 2009, pp. 5665–5671.
[17] A. Hadi, M. Abdollahi, K. Alipour, and B. Tarvirdizadeh, "Design and prototyping a new add-on module to increase traction force of a wheeled sewer inspection robot," in *Proc. 5th RSI Int. Conf. Robot. Mechatronics (ICRoM)*, Tehran, Iran, Oct. 2017, pp. 254–259.
[18] M. Kamata, K. Tachibana, Y. Tanise, T. Kawaguchi, Y. Yamada, and T. Nakamura, "Proposal of one-inch pipe inspection robot 'PI-RO I," in *Proc. 7th IEEE Int. Conf. Biomed. Robot. Biomechatronics (Biorob)*, Aug. 2018, pp. 1315–1320.
[19] A. Kojima, M. Okui, I. Hisamichi, T. Tsuji, and T. Nakamura, "Straight-fiber-type artificial muscle deformation under pressurization," *IEEE Robot. Autom. Lett.*, vol. 4, no. 3, pp. 2592–2598, Jul. 2019, doi: 10.1109/LRA.2019.2902016.
[20] Q. Ma, G. Tian, Y. Zeng, R. Li, H. Song, Z. Wang, B. Gao, and K. Zeng, "Pipeline in-line inspection method, instrumentation and data management," *Sensors*, vol. 21, no. 11, p. 3862, Jun. 2021.
[21] G. Mills, A. Jackson, and R. Richardson, "Advances in the inspection of unpiggable pipelines," *Robotics*, vol. 6, no. 4, p. 36, Nov. 2017.
[22] T. Yamamoto, M. Konyo, and S. Tadokoro, "A high-speed locomotion mechanism using pneumatic hollow-shaft actuators for in-pipe robots," in *Proc. IEEE/RSJ Int. Conf. Intell. Robots Syst. (IROS)*, Hamburg, Germany, Sep. 2015, pp. 4724–4730.
[23] K. Miyasaka, G. Kawano, and H. Tsukagoshi, "Long-mover: Flexible tube in-pipe inspection robot for long distance and complex piping," in *Proc. IEEE/ASME Int. Conf. Adv. Intell. Mechatronics (AIM)*, Auckland, New Zealand, Jul. 2018, pp. 1075–1080.
[24] H. Heung, P. W. Y. Chiu, and Z. Li, "Design and prototyping of a soft earthworm-like robot targeted for GI tract inspection," in *Proc. IEEE Int. Conf. Robot. Biomimetics (ROBIO)*, Qingdao, China, Dec. 2016, pp. 497–502.
[25] B. Zhang, Y. Fan, P. Yang, T. Cao, and H. Liao, "Worm-like soft robot for complicated tubular environments," *Soft Robot.*, vol. 6, no. 3, pp. 399–413, Jun. 2019.
[26] H. Sato, Y. Mano, F. Ito, T. Yasui, M. Okui, R. Nishihama, and T. Nakamura, "Proposal for pipeline-shape measurement method based on highly accurate pipeline length measurement by IMU sensor using peristaltic motion characteristics," in *Proc. IEEE/ASME Int. Conf. Adv. Intell. Mechtron. (AIM)*, Jul. 2020, pp. 874–881.
[27] A. Oyama, H. Iida, Y. Ji, K. Umeda, Y. Mano, T. Yasui, and T. Nakamura, "Three-dimensional mapping of pipeline from inside images using earthworm robot equipped with camera," in *Proc. 1st IFAC Workshop Robot Control (WROCO)*, Nov. 2019, vol. 52, no. 22, pp. 87–90.

F. ITO (Graduate Student Member, IEEE) received the B.S. and M.S. degrees in engineering from Chuo University, Tokyo, Japan, in 2019 and 2021, respectively.

He was a Student at the Biomechatronics Laboratory, Chuo University, from 2019 to 2020.

Dr. Ito was a recipient of the IEEE Robotics and Automation Society Japan Joint Chapter Young Award in IEEE/RSJ International Conference on Intelligent Robots and Systems (IROS 2019), in 2019.

K. TAKAYA received the B.S. degree in engineering from Chuo University, Tokyo, Japan, in 2020.

He was a Student with the Biomechatronics Laboratory, Chuo University, from 2019 to 2021.

M. KAMATA received the B.S. and M.S. degrees in engineering from Chuo University, Tokyo, Japan, in 2016 and 2018, respectively.

He was a Student at the Biomechatronics Laboratory, Chuo University, from 2017 to 2019. Since 2019, he has been working as an Engineer at Olympus Corporation.

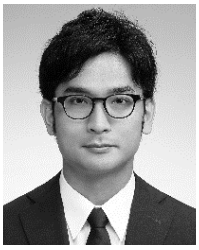

M. OKUI (Member, IEEE) received the B.S. and M.S. degrees in engineering from Tokyo Institute of Technology, Tokyo, Japan, in 2012 and 2014, respectively, and the Ph.D. degree in mechanical engineering from Chuo University, Tokyo, in 2018.

From 2014 to 2015, he worked as a Control Engineer at Nissan Motor Company Ltd. From 2016 to 2018, he was a Research Assistant with the Research and Develop Initiative, Chuo University. From 2018 to 2019, he was an Assistant Professor with the Research and Develop Initiative, Chuo University. Since 2019, he has been working as an Assistant Professor with the Faculty of Science and Engineering, Chuo University.

Y. YAMADA (Member, IEEE) received the B.S., M.S., and Ph.D. degrees from Keio University, Japan, in 2009, 2011, and 2013, respectively.

From 2013 to 2014, he was a Postdoctoral Researcher at Tokyo Institute of Technology and Keio University. He was an Engineer at Nissan Motor Company Ltd., from 2014 to 2015. He worked as an Assistant Professor at Chuo University, Tokyo, from 2015 to 2018. He was also a Visiting Assistant Professor with Dyson School of Design Engineering, Imperial College London, in 2018. Since 2019, he has been an Associate Professor with the Faculty of Engineering and Design, Hosei University. He is currently working as a CTO at Solaris Inc. His research interest includes development.

T. NAKAMURA (Member, IEEE) was born in 1975. He received the B.S. and M.S. degrees in mechanical engineering from Akita University, Akita, Japan, in 1997 and 1999, respectively, and the Ph.D. degree from Shinshu University, Nagano, Japan, in 2003.

From 1999 to 2003, he was as a Research Associate at Akita Prefecture University, Akita. In 2004, he was a Lecturer with the Faculty of Science and Engineering, Chuo University, Tokyo, Japan. From 2006 to 2013, he was an Associate Professor with Chuo University, where he has been working as a Professor, since 2013. From 2012 to 2013, he worked as a Visiting Professor with the Swiss Federal Institute of Technology, EPFL, Lausanne, Switzerland. He is the current CEO of Solaris Inc. His research interests include development and control, such as an artificial muscle, functional fluid, and development and applications of biorobotics.